ISSN (Print) 1226-1750
ISSN (Online) 2233-6656
Journal of Magnetics 26(3), 256-264 (2021) https://doi.org/10.4283/JMAG.2021.26.3.256

Structural and Magnetic Properties of Cr-doped SnO_2 Nanocrystalline Powders Based Dilute Magnetic Oxides

Kwanruthai Wongsaprom[1]*, Akekapol Winyayong[1], Supree Pinitsoontorn[2], Pinit Kidkhunthod[3], Somchai Sonsupap[4], and Santi Maensiri[4]

[1]*Physical Materials Science Unit Research, Department of Physics, Faculty of Science, Mahasarakham University, Mahasarakham 44150, Thailand*
[2]*Institute of Nanomaterials Research and Innovation for Energy (IN-RIE), Khon Kaen University, Khon Kaen 40002, Thailand*
[3]*Synchrotron Light Research Institute (Public Organization), 111 University Avenue, Muang District, Nakhon Ratchasima 30000, Thailand*
[4]*School of Physics, Institute of Science, Suranaree University of Technology Nakhon Ratchasima, 30000, Thailand*

(Received 21 December 2020, Received in final form 12 September 2021, Accepted 15 September 2021)

The nanocrystalline powders of Cr-doped SnO_2 with Cr-dopant concentrations of 2, 4 and 6 wt%, were synthesized by a simple hydrothermal method. XRD results, along with the FT-IR and SAED patterns, confirmed the formation of the SnO_2's tetragonal phase without other impurity phases. Optical analysis revealed a significant decrease in the energy gap of the doped samples from 3.69 to 3.40 eV. X-ray absorption spectroscopy, including x-ray absorption near-edge spectroscopy, was used to qualitatively investigate the valence states of doped Cr. Room temperature ferromagnetism was observed in Cr-doped SnO_2 samples. The highest value of magnetization was found in SnO_2 doped with 4 wt% of Cr (about 4.88 memu/g) and decreased slightly as the Cr concentration increased. The reduction of magnetization with the increase of Cr content happened because antiferromagnetic Cr-O-Cr super-exchange interaction took place within the nearest Cr^{3+} ions through O^{2-} ions. The oxygen vacancies were induced by the ferromagnetism in the Cr-doped SnO_2 nanocrystalline powders.

Keywords : Tin oxide, ferromagnetism, magnetic properties, dilute magnetic oxide, nanocrystalline powder

1. Introduction

In recent years, nanostructured dilute magnetic oxides (DMO) have been shown to exhibit various properties including optical transparency, wide bandgap, and ferromagnetism. When doped with a few percent of 3*d*-transition metals, DMO become ferromagnetic at and above room temperature [1-4]. Several studies on room temperature and above room temperature ferromagnetisms in 3*d*-transition metal doped oxides, such as In_2O_3 [5, 6], ZnO [8-10] and SnO_2 [11-15], have been reported. Among the metal oxides, tin oxide (SnO_2) has a wide range of applications in sensors, transparent conducting electrodes, transistors, superconductors and optoelectronic devices. SnO_2 has many desirable properties including optical transparency, wide bandgap (3.6 eV), thermal and electrochemical stabilities, nontoxicity, good biocompatibility [16, 17]. Many studies have shown the existence of ferromagnetism in Co-, Ni-, Fe-, Mn- and Cr-doped SnO_2 [2, 18-21]. Srinivas et al. [18] reported room temperature ferromagnetism for Co-doped SnO_2 nanocrystalline powders prepared by the tartaric acid gel route. Nanocrystalline powders having their size in the range of 18-50 nm were in a single phase of the tetragonal rutile structure. The powders were ferromagnetic with the magnetization of 7.2-54.3 memu/g. The authors suggested that the ferromagnetism in Co-doped SnO_2 nanocrystalline powders originated from surface diffusion of Co ions, the distribution of defects and nanometric size of materials. Ahmed *et al.* [2] reported the ferromagnetic behavior for doping of Ni-ion-doped SnO_2 nanoparticles synthesized by a sol-gel method. The authors suggested that the ferromagnetic ordering can be explained by the creation of free charge carriers and oxygen vacancies from substitution of Ni dopant into the host SnO_2 lattice. Through

*Corresponding author: Tel: +6643754379
Fax: +6643754379, e-mail: wkwanruthai@gmail.com

studies of different 3*d*-transition metal doping of SnO_2, chromium is advantageous because of its high spin configuration and a wide range of oxidation states. Furthermore, relatively small ionic radius difference between Cr ions and Sn^{4+} facilitates the incorporation of Cr dopant into the host SnO_2 lattice. The origin of ferromagnetic ordering of Cr-doped SnO_2 nanostructures is still contentious. There are only a few reports on Cr- doped SnO_2 nanostructures. Zhang *et al.* [21] reported the ferromagnetism on Cr-doped SnO_2 nanowires with the highest magnetization of 0.104 emu/g. The magnetization value decreased with increasing dopant concentration. The authors suggested that the intrinsic ferromagnetism arises from oxygen vacancies and the coupling between the unpaired electrons of Cr. Kusuma *et al.* [3] reported the solubility limit of Cr^{3+} dopant in SnO_2 nanoparticles synthesized by a non-equilibrium solution combustion method. The authors found that the magnetization decreased drastically in nanoparticles at > 2% Cr-doped SnO_2. In addition, the ferromagnetic properties of Cr-doped SnO_2 nanoparticles have been demonstrated in materials synthesized by a chemical co-precipitation method capped with polyethylene glycol (PEG). They suggested that the capping agents of PEG were necessary to provide chemical passivation and to improve the surface state which has significant influence on the properties of nanoparticles [3]. In view of this, it is clear that the ferromagnetic ordering in oxide materials is highly dependent on the conditions of processing and the synthesis method adopted. Therefore, in the light of this understanding, we investigated systematically the influence of Cr-doping level on the structural, morphological, optical and magnetic properties of SnO_2 nanocrystalline powders. The nanocrystalline powders of Cr-doped SnO_2 with a chromium concentration of 0 to 6 wt% were synthesized by a simple hydrothermal method. Such studies will give a good understanding for spintronic applications.

2. Experimental Procedure

In this study, SnO_2 and Cr-doped SnO_2 nanostructures were synthesized by a simple hydrothermal method using high purity tin chloride ($SnCl_2{\cdot}2H_2O$) and chromium nitrate nonahydrate ($CrN_3O_9{\cdot}9H_2O$) as starting materials. We investigated how different Cr concentrations influenced ferromagnetism and the solubility limit of Cr ion in SnO_2 structures. When doping of Cr was further increased to 6 wt%, the ferromagnetism decreased. Therefore, four samples with 0 wt%, 2 wt%, 4 wt% and 6 wt% concentrations of chromium nitrate nonahydrate were prepared. In a typical procedure, a 0.1 M solution of $SnCl_2{\cdot}2H_2O$ with various concentrations of $CrN_3O_9{\cdot}9H_2O$ was prepared using deionized water as a solvent. The mixed solution of 0.1 M tin chloride and chromium nitrate nonahydrate with different Cr (0, 2, 4 and 6 wt%) content was stirred with magnetic stirrer at room temperature for 2 h. Then sodium hydroxide (NaOH) was added dropwise to the solution until the pH reached 12. The homogeneous solution was transferred into a Teflon-lined stainless-steel autoclave, sealed and maintained at 200 ^oC for 12 h. After the autoclave was cooled to room temperature. The precipitate was collected and washed several times separately with deionized water and ethanol. The product was then dried in a vacuum at 70 ^oC overnight. The final product obtained was white SnO_2 powder. The samples were characterized for crystal phase identification by powder x-ray diffraction (XRD) using a D8 Advance X-ray (Buker, German) with CuKα radiation (λ = 0.15418 nm). The Fourier transform infrared (FT-IR) spectra of the powders (as pellets in KBr) were recorded using a Fourier transform infrared spectrometer (Spectrum GX FT-IR spectrometer, Perkin Elmer Instruments, England). Morphological analysis and characterization of the samples employed transmission electron microscopy (TEM) (Hitachi H8100 200 kV) equipped with an energy dispersive x-ray spectrometer (EDX). The optical absorption spectra were measured using a UV-vis spectrometer (UV-3101PC, Shidamazu, Japan). X-ray absorption near edge structure (XANES) spectra of Cr *K*-edge were measured in transmission mode using a Ge(220) double-crystal monochromator with an energy resolution ($\Delta E/E$) of 2×10^{-4} at the SUT-NANOTEC-SLRI XAS Beamline (BL 5.2) (electron energy of 1.2 GeV; bending magnet; beam current 80-150 mA; 1.1 to 1.7×10^{11} photon s^{-1}). Additionally, XANES spectra of known decisive oxidation state of Cr metal, Cr_2O_3 (Cr^{3+}) and CrO_3 (Cr^{6+}) samples were measured for comparison. The magnetic measurements were performed at room temperature using a vibrating sample magnetometer (Versa Lab VSM, Quantum Design).

3. Results and Discussion

XRD was used to determine the structure of SnO_2 and Cr-doped SnO_2 samples as showed in Fig. 1. The samples revealed the tetragonal structure of SnO_2 when compared to the standard data (JCPDS 41-1445). The XRD pattern of the Cr-doped samples indicated that Cr ions might be substituted into the SnO_2 lattice. There were no diffraction peaks corresponding to Cr-related secondary phases observed in the Cr-doped samples. This result confirms the substitution of Sn^{4+} ions by Cr ions in the nanostructure of doped samples [22]. The crystallite size of

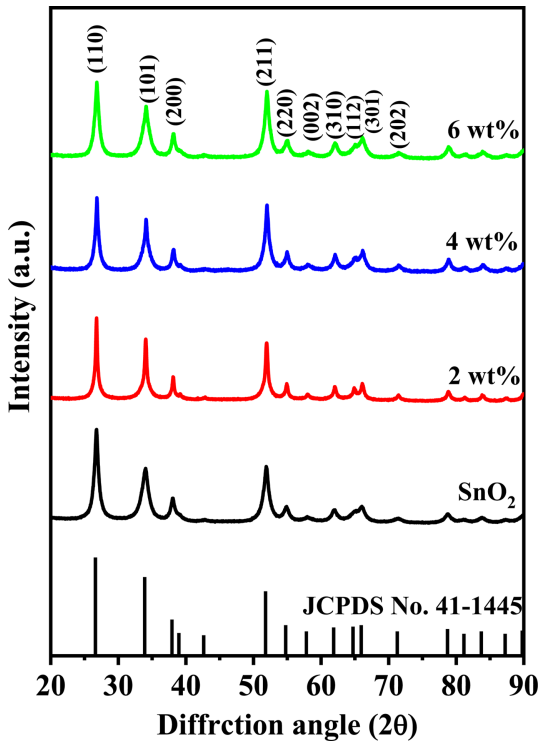

Fig. 1. (Color online) XRD patterns of SnO_2 and Cr-doped SnO_2 nanostructures.

SnO_2 samples was calculated from x-ray line broadening of the peak at (110), (101) and (211) planes using Scherrer's equation [23]. The crystallite size obtained was 9.8 ± 1.6 nm. Figure 2 shows XRD patterns with full Rietveld refinement analysis for SnO_2 and Cr-doped SnO_2 samples. Rietveld refinement demonstrated that the samples were consistent with the tetragonal structure of SnO_2 without any detectable secondary phases of chromium oxides (Cr_2O_3, Cr_3O_4 and CrO_3) or another mixed tin oxide (SnO and Sn_2O_4). The lattice parameters and the volume of unit cell for Cr-doped SnO_2 nanostructures were found to be slightly smaller than the pure SnO_2 sample as summarized in Table 1. A small decrease in the volume of unit cell for Cr-doped SnO_2 samples is expected for a successful substitution of Sn ions by Cr ions in the samples because the radius of Cr ions is slightly smaller than the radius of Sn^{4+} ions. These results are in good agreement with the values reported by other research groups [21, 22].

The functional groups and the types of chemical bonds of the SnO_2 and Cr-doped SnO_2 nanostructures were determined by FT-IR as presented in Fig. 3. It is clear from the figure that there were clear changes in the intensity and shapes of IR peaks indicating that Cr might have been incorporated into the SnO_2 structure. The absorption bands at ~3452, 3142 and 1633 cm^{-1} have been assigned to the vibration of hydroxyl groups from absorbed water on surface of the samples and to a stretching vibrational mode of O-H groups, respectively [22, 24, 25]. The peak at ~2372 cm^{-1} was assigned to the absorption of atmospheric carbon dioxide with water [26]. The band located at ~ 1395 and 1238 cm^{-1} corresponded to C=O and C-C bonds respectively [27, 28]. In addition, the band in range 400-1000 cm^{-1} can be attributed to a vibration of metal oxide bonds. The band appearing at 951 cm^{-1} can be assigned to the Sn-O antisymmetric vibration. The band around 649 cm^{-1} was ascribed to the antisymmetric Sn-O-Sn stretching mode of the surface-bridging oxide [29], while the band at 530 cm^{-1} was due to Sn–OH bonds of the SnO_2 crystalline phase [30]. Metal oxide generally reveals absorption bands below the 1000 cm^{-1} region [31, 32]. Therefore, the band with stretching mode at ~951, 649 and 530 cm^{-1} corresponded with the formation of SnO_2 tetragonal structure in the samples as well as the result from XRD technique. The analysis of FT-IR spectra of SnO_2 and Cr-doped SnO_2 samples proved that the tetragonal of SnO_2 crystal structure were obtained through the hydrothermal method.

The morphology and structure of SnO_2 and Cr-doped SnO_2 samples was investigated by obtaining TEM by bright field images and performing selected area electron diffraction (SAED). TEM image of SnO_2 sample showed agglomerated nanoparticles with particle size around 13.5 nm as shown in Fig. 4(a). The SAED pattern of the sample reveals spotty ring patterns of tetragonal structure of

Table 1. Summary of particle size from TEM, lattice constant a, c, unit cell volume (V) from the refinement of XRD patterns and saturation magnetization (M_s) of SnO_2 and Cr-doped SnO_2 nanostructures.

Samples	Particle size (nm)		Lattice parameter			M_s (memu/g)	E_g (eV)
	from TEM		a (nm)	c (nm)	V $(nm)^3$		
	Spherical shape	Rod shape					
SnO_2	13.5	-	0.4762(7)	0.3198(3)	0.0725(5)	dia	3.69
2 wt%	12.6	31.6 (length) 5.6 (width)	0.4746(8)	0.3195(4)	0.0720	1.73	3.57
4 wt%	12.4	30.5 (length) 5.0 (width)	0.4738(4)	0.3194(5)	0.0717(2)	4.88	3.42
6 wt%	12.3	32.8 (length) 3.8 (width)	0.4730(6)	0.3182(0)	0.0712(1)	para	3.40

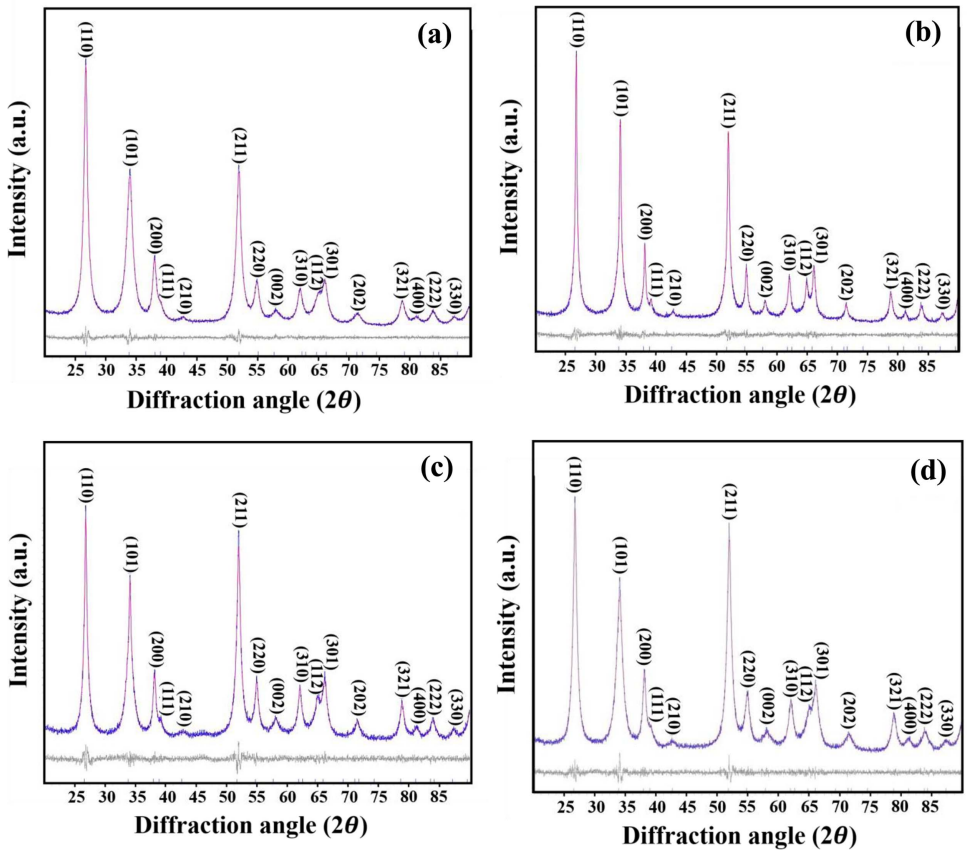

Fig. 2. (Color online) Rietveld refined XRD patterns of pure and doped SnO_2 with various Cr contents (a) 0 wt%, (b) 2 wt%, (c) 4 wt% and (d) 6 wt% samples.

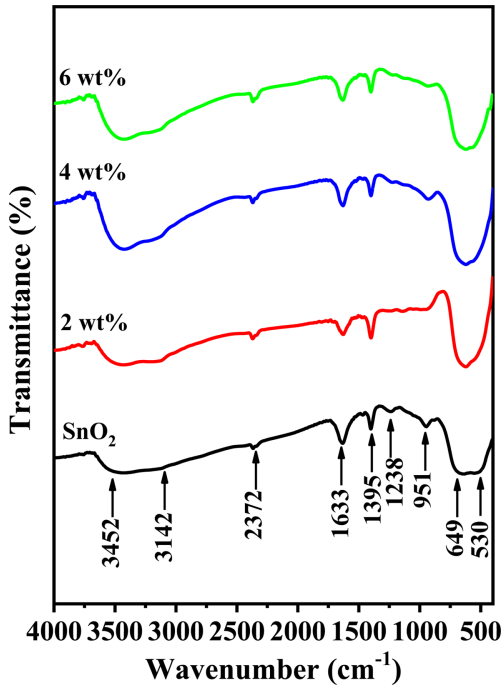

Fig. 3. (Color online) FT-IR spectra of pure and doped SnO_2 with various Cr contents (a) 0 wt%, (b) 2 wt%, (c) 4 wt% and (d) 6 wt% nanostructures.

SnO_2. The high-resolution TEM image in Fig. 4(c) reveals the details of the SnO_2 nanoparticles with the measured spacing of the lattice fringe of 0.3237 nm corresponding to the (110) plane of SnO_2. Figure 4(d), 4(g) and 4(j) display TEM images of 2 wt%, 4 wt% and 6 wt% Cr-doped SnO_2 samples, respectively. The results show the mixed morphologies of the rod and spherical shapes. The sizes of nanorods was around 3.8-5.6 nm in width and 30.5-32.8 nm in length. The sizes of nanoparticles was around 12.3-12.6 nm. The nanoparticles' sizes of the doped samples decreased when the concentration of Cr was increased as summarized in Table 1. Similar results have also been reported by Lavanya *et al.* [33] and Aquino *et al.* [34]. The SAED patterns show spotty ring patterns of tetragonal structure of SnO_2 without any additional diffraction spots and rings of Cr based secondary phases in agreement with the XRD results and standard data (JCPDS: 41-1445). As shown in Fig. 4(f), 4(i) and 4(l), the spacing of the lattice fringes from high-resolution TEM images of the 2 wt%, 4 wt% and 6 wt% Cr-doped SnO_2 samples were measured to be ~0.2538, 0.1886 and 0.2658 nm, respectively. These spacings correspond to the

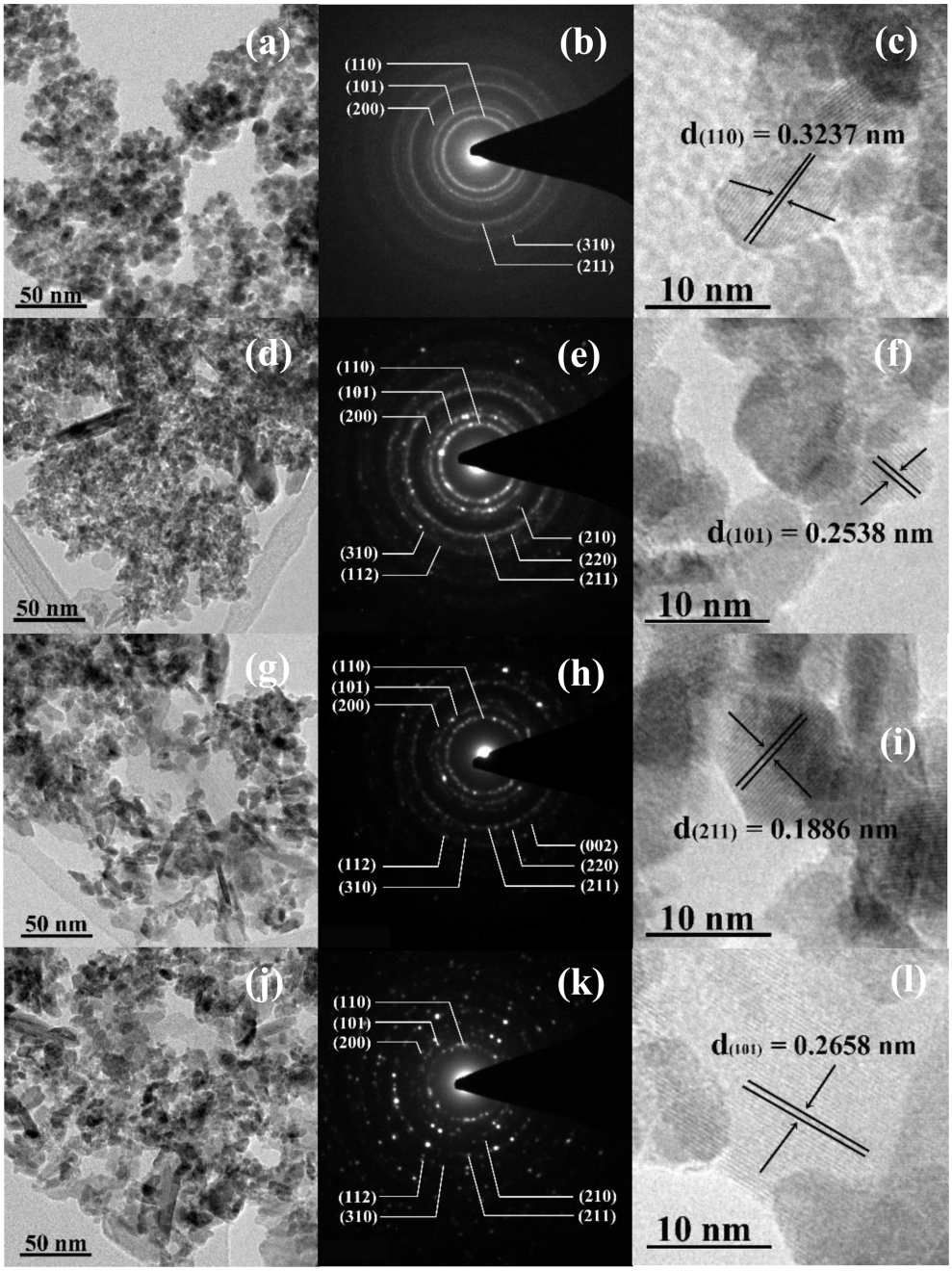

Fig. 4. Magnetization of (a) SnO_2 and (b) 2 wt% and 4 wt% Cr-doped SnO_2 nanostructures at 300 K. The inset in (b) of top left shows the magnetization of 6 wt% and bottom right shows the low-field magnetization of 4 wt% Cr-doped SnO_2 nanostructures.

(101), (211) and (101) planes of SnO_2. The elemental composition and quantitative analysis were investigated by EDX in TEM. EDX data reveal that the pure SnO_2 sample had peaks for Sn and O, while the peaks for Cr were present in the Cr-doped samples as presented in Fig. 5. This may be due to the substitution of Cr ions for Sn on the SnO_2 structure or impurity phases of Cr. However, no evidence of impurity phases was identified by XRD and TEM. The quantitative analysis revealed the average Cr doping concentration in the dopant samples was 2.61 wt%, 4.21 wt% and 6.22 wt% for the 2 wt%, 4 wt% and 6 wt% Cr-doped samples, respectively. Moreover, the presence of Cu resulted from copper grid contamination.

The UV-vis absorption spectra of pure and Cr-doped SnO_2 samples are shown in Fig. 6. It can be seen from the figure that doping with Cr resulted in a red shift of the photophysical responses of pure SnO_2 nanoparticles. The absorption in the UV-visible region was increased by

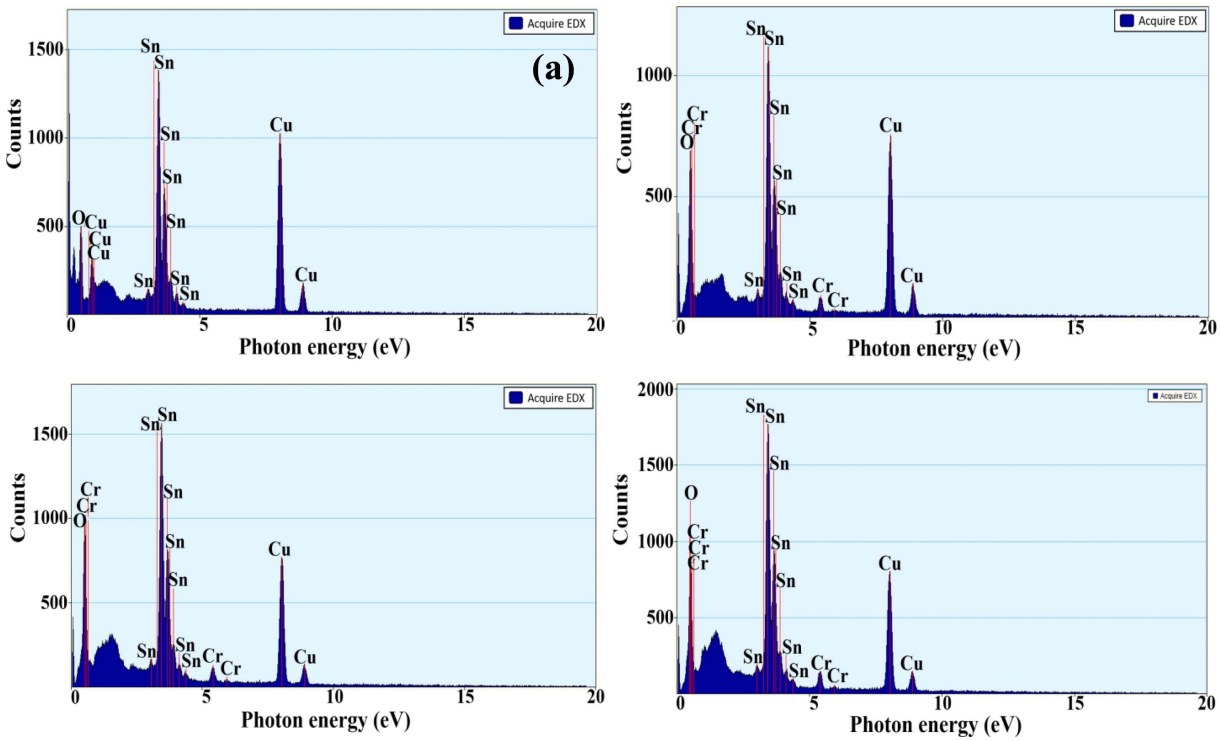

Fig. 5. (Color online) EDX patterns of (a) 0 wt%, (b) 2 wt%, (c) 4 wt% and (d) 6 wt% Cr-doped SnO_2 nanostructures.

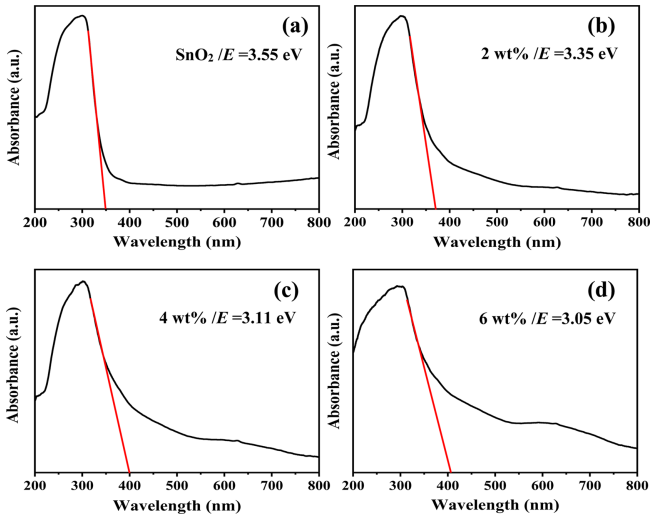

Fig. 6. Optical absorbance spectra of SnO_2 and 2 wt%, 4 wt% and 6 wt% Cr-doped SnO_2 nanostructures.

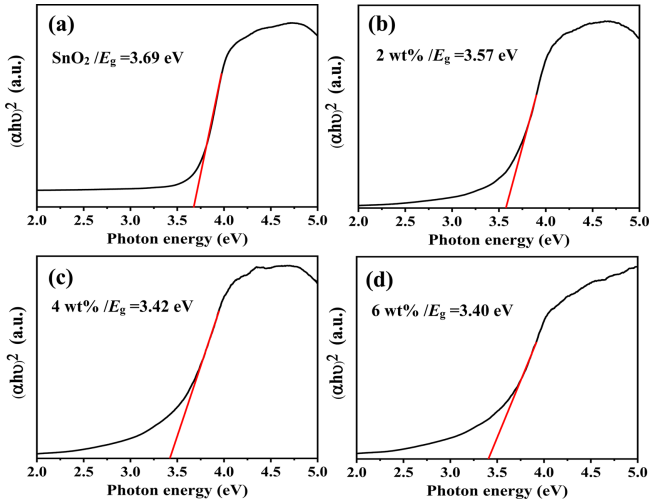

Fig. 7. (Color online) Plot of $(\alpha h\nu)^2$ as a function of photon energy of (a) 0 wt%, (b) 2 wt%, (c) 4 wt% and (d) 6 wt% Cr-doped SnO_2 nanostructures.

increasing the concentration of Cr dopant. The absorption spectra show strong cut-off at 350 nm (3.55 eV), 371 nm (3.35 eV), 399 nm (3.11 eV) and 406 nm (3.05 eV), for pure and 2 wt%, 4 wt% and 6 wt% Cr-doped samples, respectively. The optical band gap of the samples can be obtained by extrapolating the linear portion of the plot $(\alpha h\nu)^2$ versus hν [35, 36]. As displayed in Fig. 7, the extrapolations of the linear portion of the curves toward zero absorbance (y=0) give E_g for direct transitions. The estimated optical band gap energy decreased as the Cr dopant level increased. The band gap for pure sample was 3.69 eV. The band gap decreases to the lowest value of 3.40 eV for 6 wt% Cr-doped sample. This result is close to that reported in the literature [2, 18]. The decrease of the estimated value of the band gap in Cr-doped samples can be explained by the doping of Cr ions into SnO_2

lattice that can introduce defective energy levels into the band gap of SnO_2. The new energy states are located within the gap of SnO_2 for electron-hole pair recombination with lower energy [2]. This process can effectively lower the band edge adsorption threshold of SnO_2. The redshift of the band gap in this system can be attributed to *s-d* and *p-d* exchange interactions between the band electrons of SnO_2 and the localized *d* electrons of Cr ions substituting Sn ions [37, 38]. In addition, the reduction of band gap can be induced by the presence of oxygen vacancies located in the samples [14].

In order to determine the valence state of Cr atoms in the doped samples, we performed x-ray absorption near edge structure (XANES) of Cr *K*-edge studies of our samples. The XANES spectra at Cr *K*-edge were measured in transmission mode at room temperature at the BL5.2 station. Figure 8 shows XANES spectra for Cr-doped SnO_2 samples and reference spectra for Cr metal (Cr atom), Cr_2O_3 (Cr^{3+}) and CrO_3 (Cr^{6+}). Figure 8(a) shows the absorption pre-edge energy of the Cr-doped SnO_2 samples that are closed Cr_2O_3 (5999.70 eV) indicate that oxidation state of Cr^{3+} in structures. Also, Fig. 8(c) reveals the edge of Cr spectra of all samples was matched to the edge energy of Cr_2O_3. This result implies that the Cr ion substitution of Sn^{4+} ion into the SnO_2 lattice has an oxidation state of +3. To understand more about the edge positions and features of the samples, the first derivative absorption (Fig. 8(b) and 8(d)) was analyzed. From the first derivative absorption result, when considering the pre-edge position of samples, we found that the position was 5989.24, 5989.30 and 5989.27 eV confirm the pre-edge energy position are Cr^{3+} in the samples. Moreover, the edge position of standard (Cr_2O_3 = 6003.84 eV) is very close to the edge energy of all samples (6003.49 eV), this result indicates that Cr valence state in the samples has certain values is +3 [39]. Therefore, additional studies were conducted and found that the XANES spectra of samples were very similar to the XANES spectrum of Cr_2O_3 (Cr^{3+}). The presence of this feature in

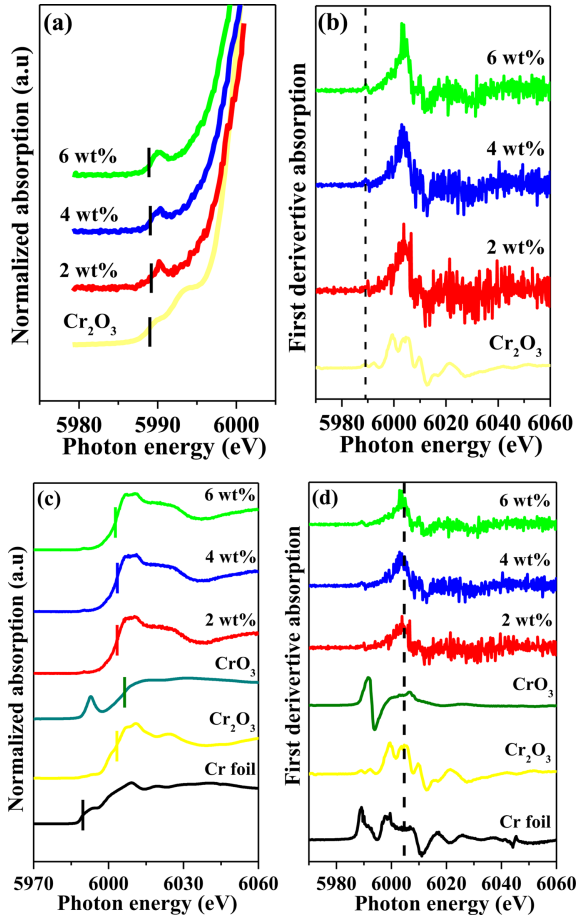

Fig. 8. (Color online) (a), (c) XANES spectra pre-edge and edge spectra at Cr (*K*-edge) of Cr metal Cr_2O_3 (Cr^{3+}), CrO_3 (Cr^{6+}) standards and (b), (d) first derivative of the Cr *K*-edge XANES spectra of samples.

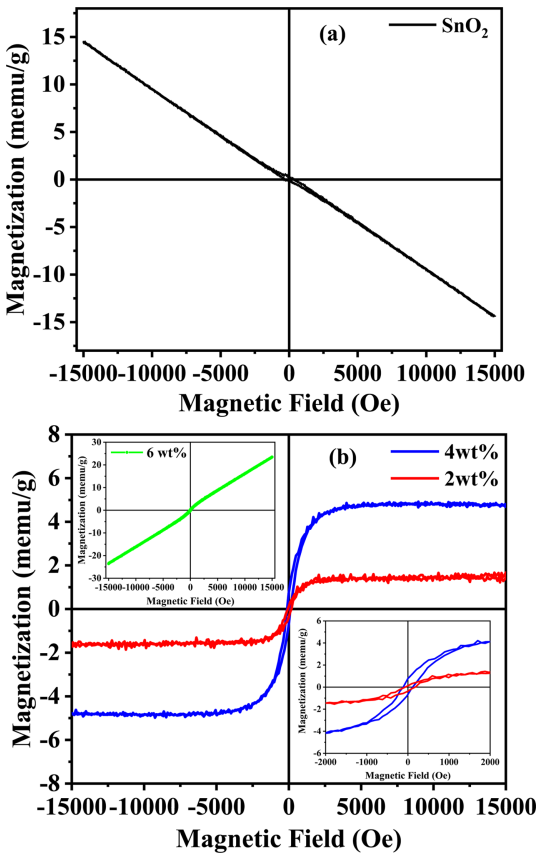

Fig. 9. (Color online) Magnetization of (a) SnO_2 and (b) 2 wt% and 4 wt% Cr-doped SnO_2 nanostructures at 300 K. The inset in (b) of top left shows the magnetization of 6 wt% and bottom right shows the low-field magnetization of 4 wt% Cr-doped SnO_2 nanostructures.

the spectra of all doped samples implies that there was a substitution of Sn^{4+} ions by Cr^{3+} ions. Therefore, in this research, we demonstrate that the Cr^{3+} ions replaced the Sn^{4+} ions in the SnO_2 structure.

Magnetization curves for the pure and Cr-doped samples were measured at 300 K as shown in Fig 9. Figure 9(a) shows the diamagnetic behavior of the pure SnO_2 was in good agreement with the literature [2, 40]. The diamagnetic behavior for the SnO_2 sample may be due to the valence state of tin (Sn^{4+}) in which the $4d^{10}$ electron configuration of Sn is present in SnO_2. The samples have the saturation magnetization of about 1.73 and 4.88 memu/g for 2 wt% and 4 wt% Cr contents (Table 1). The magnetization slightly increased with increased chromium content. However, the sample doped with 6 wt% Cr is linear and there is no hysteresis. This indicates that the sample was not ferromagnetic, as shown in the inset of Fig. 9(b). The drop of magnetization in the sample came from any antiferromagnetic Cr-O-Cr super exchange interaction taking place within the nearest Cr^{3+} ions through O^{2-} ions. In addition, an increase in Cr concentration may lead to the reduction of the interdistance between Cr-Cr pair inducing an antiferromagnetic exchange, which may dominate over ferromagnetic interaction in the 6 wt% Cr-doped sample. Similar results have been reported by other researchers [3, 15, 41]. Hence, these antiferromagnetic exchange interactions should exist in the 6 wt% Cr-doped SnO_2 nanostructures. The ferromagnetism in Cr-doped SnO_2 system may have originated from several mechanisms that induced a different magnitude of the magnetic moment at the same time (they may relate to defect, oxygen vacancy, metallic Cr clusters, etc) [4, 41]. However, XRD, Rietveld refinement and SAED studies have not observed the presence of impurity and magnetic phases in the Cr-doped SnO_2 samples. The results of XANES confirmed that the Cr ions in SnO_2 were Cr^{3+} ions. The Cr^{3+} ion substitution for Sn^{4+} ion in the SnO_2 lattice results in the creation of oxygen vacancies in order to ensure charge neutrality [42, 43]. Several groups of researchers have calculated and experimented with a ferromagnetically ordered components due to oxygen vacancies for SnO_2 and Cr-doped SnO_2 systems [13-15, 41, 42, 44]. A comparison of the effect of oxygen vacancy for SnO_2 by annealing under oxygen atmosphere revealed that the sample lost its ferromagnetic properties, and became to diamagnetically ordered [14]. Studies on Cr concentration and annealing under oxygen-rich or vacuum atmospheres have been reported in Cr-doped SnO_2 systems [41]. The authors found that the oxidizing atmosphere compensated the oxygen vacancy in the sample and induced the disappearance of ferromagnetism. However, the vacuum annealing resulted in the increase of the oxygen vacancy, which induced the ferromagnetic ordering. Paul *et al.* [45] reported the ferromagnetism of Ni^{2+}-doped SnO_2 decreased and the paramagnetism returned when annealing was performed at low temperature. The authors suggested that the defects play an important role in ferromagnetism of SnO_2. These reports are similar to our results. We consider, the ferromagnetic mechanism in our samples may originate from the presence of oxygen vacancy. This point can be explained by F-centre mediated exchange mechanism in dilute magnetic oxide materials using a bound magnetic polaron (BMP) model [46]. This result is in good agreement previous reports in the literature [10, 17, 21, 47, 48] for Ni^{2+}-/Co^{2+}-/Cr^{3+}-/Mn^{3+}-/Cu^{2+}-doped SnO_2 systems. However, the method and condition of fabrication are also related to magnetic properties and oxygen stoichiometry for SnO_2 system.

4. Conclusion

Nanocrystalline powders of pure and Cr-doped SnO_2 with particle size of ~12-13 nm have been successfully synthesized by a hydrothermal method. The samples with different Cr content demonstrated room temperature ferromagnetism and had a pure phase of tetragonal. The reduction of band gap may have been related to the presence of oxygen vacancies in the Cr-doped SnO_2 structure. The origin of ferromagnetism in this system may be explained by F-centre exchange due to the presence of an oxygen vacancy through carrier mediated polaron interaction. However, at the solubility limit of Cr dopant (6 wt%), an antiferromagnetic exchange may have dominated over the ferromagnetic interaction and decreased the magnetization in the sample.

Acknowledgments

The authors would like to thank the Synchrotron Light Research Institute (BL5.2) (Public Organization), Nakhon Ratchasima, Thailand for XAS, and the Department of Physics, Khon Kaen University for providing VSM facilities. This research project was financially supported by Thailand Research Fund (Contact No. MRG6080262).

References

[1] J. M. D. Coey, Curr. Opin. Solid St. M. **10**, 83 (2006).
[2] A. Ahmed, T. Ali, M. Naseem Siddique, A. Ahmad, P. Tripathi, J. Appl. Phys. **122**, 083906 (2017).
[3] K. Urs, S. V. Bhat, and V. Kamble, J. Appl. Phys. **123**, 161518 (2018).

[4] N. H. Hong, J. Sakai, W. Prellier, and A. Hassini, J. Phys.: Condens. Matter **17**, 1697 (2005).
[5] K. Wongsaprom, R. Jareanboon, S. Kingcha, S. Pinitsoontorn, and W. Ponhan, J. Supercond. Nov. Magn. **30**, 1053 (2017).
[6] S. Yan, S. Ge, Y. Zuo, W. Qiao, and L. Zhang, Scripta Mater. **61**, 387 (2009).
[7] N. H. Hong, J. Sakai, N. Poirot, and V. Briz, Phys. Rev. B **73**, 132404 (2006).
[8] B. Martinez, F. Sadiumenge, L. I. Balcells, J. Arbiol, F. Sibieude, and C. Monty, Appl. Phys. Lett. **86**, 103113 (2005).
[9] S. Zhao, Y. Bai, J. Chen, A. Bai, and W. Gao, J. Magn. **19**, 68 (2014).
[10] N. H. Hong, J. Sakai, and V. Brizé, J. Phys.: Condens. Matter **19**, 036219 (2007).
[11] S. Mohanty and S. Ravi, Solid State Commun. **150**, 1570 (2010).
[12] S. Mehraj and M. Shahnawaze Ansari, Physica E **65**, 84 (2015).
[13] N. H. Hong, N. Poirot, and J. Sakai, Phys. Rev. B **77**, 033205 (2008).
[14] G. S. Chang, J. Forrest, E. Z. Kurmaev, A. N. Morozovska, M. D. Glinchuk, J. A. McLeod, A. Moewes, T. P. Surkova, and N. H. Hong, Phys. Rev. B **85**, 165319 (2012).
[15] A. Sundaresan, R. Bhargavi, N. Rangarajan, U. Siddesh, and C. N. R. Rao, Phys. Rev. B **74**, 161306(R) (2006).
[16] S. Das and V. Jayaraman, Prog. Mater. Sci. **66**, 112 (2014).
[17] V. Agrahari, M. Chandra Mathpal, M. Kumar, and A. Agarwal, J. Alloys Compd. **622**, 48 (2015).
[18] K. Srinivas, M. Vithal, B. Sreedhar, M. Manivel Raja, and P. Venugopal Reddy, J. Phys. Chem. C **113**, 3543 (2009).
[19] L. Fang, X. Zu, C. Liu, Z. Li, G. Peleckis, S. Zhu, H. Liu, and L. Wang, J. Alloys Compd. **491**, 679 (2010).
[20] N. Ahmad, S. Mohd, and M. N. Ansari, Ceram. Int. **44**, 15972 (2018).
[21] L. Zhang, S. Ge, Y. Zuo, J. Wang, and J. Qi, Scripta Mater. **63**, 953 (2010).
[22] K. Subramanyam, N. Sreelekha, G. Murali, D. A. Reddy, and R. P. Vijayalakshmi, Phys. B Condens. Matter. **454**, 86 (2014).
[23] B. D. Cullity and S. R. Stock, Elements of X-ray Diffraction, 3nd ed., Printice Hall, New Jersey, 388 (2001).
[24] D. L. Chen and L. Gao, J. Colloid Interf. Sci. **279**, 137 (2004).
[25] J. R. Zhang and L. Gao, Inorg. Chem. Commun. **7**, 91 (2004).
[26] B. Nandan, B. Venugopal, S. Amirthapandian, B. K. Panigrahi, and P. Thangadurai, J. Nanopart. Res. **15**, 1999 (2013).
[27] A. K. Mishra and D. Das, Mater. Sci. Eng. B **171**, 5 (2010).
[28] R. K Dutta, P. K. Sharma, and A. C. Pandey, J. Nanopart. Res. **12**, 1211 (2010).
[29] H. Seema, K. Christian Kemp, V. Chandra, and K. S. Kim, Nanotechnology **23**, 355705 (2012).
[30] T. Van Tran, S. Turrell, M. Eddafi, B. Capoen, M. Bouazaoui, P. Roussel, S. Berneschi, G. Righini, M. Ferrari, S. N. B. Bhaktha, O. Cristini, and C. Kinowski, J. Mol. Struct. **976**, 314 (2010).
[31] G. Vijayaprasath, R. Murugan, S. Asaithambi, G. Anandha Babu, P. Sakthive, T. Mahalingam, Y. Hayakawa, and G. Ravi, Appl. Phys. A **122**, 122 (2016).
[32] V. Rajendran and K. Anandan, Mater. Sci. Semicond. Process. **15**, 393 (2012).
[33] N. Lavanya, S. Radhakrishnan, C. Sekar, M. Navaneethan, and Y. Hayakawa, Analyst. **138**, 2061 (2013).
[34] J. Aquino, F. H. Aragon, J. A. H. Coaquira, X. Gratens, V. A. Chitta, I. J. Gonzalez, W. A. A. Macedo, and P. C. Morais, J. Phys. Chem. C **121**, 21670 (2017).
[35] A. M. J. Tauc, J. Non. Cryst. Solids. **569**, 8 (1972).
[36] E. Ziegler, A. Heinrich, H. Oppermann, and G. Stöver, Phys. Solid State **66**, 635 (1981).
[37] N. Salah, S. Habib, and A. Azam, Appl. Phys. A Mater. Sci. Process **122**, 1 (2016).
[38] K. Karthika and K. Ravichandran, J. Mater. Sci. Technol. **31**, 1111 (2015).
[39] S. Ould-Chikh, O. Proux, P. Afanasiev, L. Khrouz, M. N. Hedhili, D. H. Anjum, M. Harb, C. Geantel, J. M. Basset, and E. Puzenat, ChemSusChem. **7**, 1361 (2014).
[40] J. Hays, A. Punnoose, R. Baldner, M. H. Engelhard, J. Peloquin, and K. M. Reddy, Phys. Rev. B **72**, 075203 (2005).
[41] Y. Zuo, S. Ge, L. Zhang, S. Yan, X. Zhou, and Y. Xiao, J. Alloys Compd. **475**, 60 (2009).
[42] P. D. Borges, L. M. R. Scolfaro, H. W. Leite Alves, E. F. da Silva Jr., and L. V. C. Assali, Appl. Surf. Sci. **267**, 115 (2013).
[43] S. K. Misra, S. I. Andronenko, S. Rao, S. V. Bhat, C. V. Komen, and A. Punnoose, J. Appl. Phys. **105**, 07C514 (2009).
[44] N. H. Hong, J.-H. Song, A. T. Raghavender, T. Asaeda, and M. Kurisu, Appl. Phys. Lett. **99**, 052505 (2011).
[45] I. A. Paul and R. G. Daniel, J. Appl. Phys. **99**, 08M107 (2006).
[46] J. M. D. Coey, M. Venkatesan, and C. B. Fitzgerald, Nat. Mater. **41**, 73 (2005).
[47] Y. Xiao, S. Ge, L. Xi, Y. Zuo, X. Zhou, B. Zhang, L. Zhang, C. Li, X. Han, and Z. Wen, Appl. Surf. Sci. **254**, 7459 (2008).
[48] A. Johari, S. Srivastav, M. Sharma, and M. C. Bhatnagar, J. Magn. Magn. Mater. **362**, 1 (2014).